Mass–Radius Relations of Compact Stars in Newtonian Gravity and General Relativity

Rabia Nisa Kalkan
Department of Physics, Koç University,
Rumelifeneri Yolu, 34450 Sariyer, Istanbul, Turkey
(Dated: January 11, 2026)

We study the structure of compact stars in two regimes. In Newtonian gravity we derive the Lane–Emden equation for polytropes, convert white dwarf observations into a mass–radius relation, and fit the low-mass data with a polytropic approximation to infer an effective index and normalization. We then use a full cold white-dwarf equation of state to construct a numerical mass–radius curve and compare the resulting Chandrasekhar mass with the ultra-relativistic analytic limit. In general relativity we solve the Tolman–Oppenheimer–Volkoff equations for two polytropic equations of state, compute mass–radius and binding-energy relations, identify stability via turning points, and determine the minimum stiffness required to support a $2.5\,M_\odot$ neutron star.

INTRODUCTION

Compact stars provide a clean setting where gravity and microphysics jointly determine global observables such as mass and radius. The structure of the report and the computational workflow follow the project guidelines for the term project (Ref. [1]). First, we treat white dwarfs in Newtonian gravity using polytropes and a more realistic cold-degenerate equation of state, with direct comparison to observational data. Second, we move to neutron stars in general relativity and solve the Tolman–Oppenheimer–Volkoff (TOV) equations for two polytropic equations of state, extracting mass–radius relations, binding energies, and stability properties.

NEWTON

Lane–Emden equation and polytropic scaling

The Newtonian stellar structure equations are

$$\frac{dm}{dr} = 4\pi r^2 \rho(r), \qquad \frac{dp}{dr} = -\frac{Gm(r)\rho(r)}{r^2}, \tag{1}$$

together with the polytropic equation of state

$$p = K\rho^\gamma = K\rho^{1+\frac{1}{n}}. \tag{2}$$

We rewrite hydrostatic equilibrium as

$$\frac{1}{\rho}\frac{dp}{dr} = -\frac{Gm}{r^2}. \tag{3}$$

Multiplying by r^2 and differentiating with respect to r, we have

$$\frac{d}{dr}\left(\frac{r^2}{\rho}\frac{dp}{dr}\right) = -G\frac{dm}{dr}. \tag{4}$$

Using mass continuity, $\frac{dm}{dr} = 4\pi r^2\rho$, gives

$$\frac{d}{dr}\left(\frac{r^2}{\rho}\frac{dp}{dr}\right) = -4\pi G r^2 \rho. \tag{5}$$

We then write $\frac{dp}{dr}$ with $p = K\rho^{1+1/n}$ as

$$\frac{dp}{dr} = \frac{dp}{d\rho}\frac{d\rho}{dr} = K\left(1+\frac{1}{n}\right)\rho^{1/n}\frac{d\rho}{dr}, \tag{6}$$

so

$$\frac{1}{\rho}\frac{dp}{dr} = K\left(1+\frac{1}{n}\right)\rho^{1/n-1}\frac{d\rho}{dr}. \tag{7}$$

We introduce the dimensionless function θ

$$\theta = (\rho(r)/\rho_c)^{\frac{1}{n}}, \qquad \rho = \rho_c\theta^n \tag{8}$$

with $\rho_c = \rho(0)$. Then

$$\frac{d\rho}{dr} = \rho_c\, n\,\theta^{n-1}\frac{d\theta}{dr}, \qquad \rho^{1/n-1} = (\rho_c\theta^n)^{1/n-1} = \rho_c^{1/n-1}\theta^{1-n}, \tag{9}$$

and therefore

$$\rho^{1/n-1}\frac{d\rho}{dr} = n\,\rho_c^{1/n}\frac{d\theta}{dr}. \tag{10}$$

Hence Eq. (7) becomes

$$\frac{1}{\rho}\frac{dp}{dr} = K\left(1+\frac{1}{n}\right)n\rho_c^{1/n}\frac{d\theta}{dr} = K(n+1)\rho_c^{1/n}\frac{d\theta}{dr}. \tag{11}$$

Substituting into Eq. (5) gives

$$\frac{d}{dr}\left(r^2 K(n+1)\rho_c^{1/n}\frac{d\theta}{dr}\right) = -4\pi G r^2\rho_c\,\theta^n. \tag{12}$$

Dividing both sides by the constant $K(n+1)\rho_c^{1/n}$ gives

$$\frac{d}{dr}\left(r^2\frac{d\theta}{dr}\right) = -\frac{4\pi G\rho_c^{1-1/n}}{K(n+1)}\,r^2\,\theta^n. \tag{13}$$

We define the length scale

$$a^2 \equiv \frac{(n+1)K}{4\pi G}\,\rho_c^{1/n-1}, \tag{14}$$

so that $\frac{4\pi G\rho_c^{1-1/n}}{K(n+1)} = \frac{1}{a^2}$, and Eq. (13) becomes

$$\frac{d}{dr}\left(r^2\frac{d\theta}{dr}\right) = -\frac{r^2}{a^2}\theta^n. \tag{15}$$

Then we set $r = a\xi$ and use $\frac{d}{dr} = \frac{1}{a}\frac{d}{d\xi}$ to obtain

$$\frac{1}{\xi^2}\frac{d}{d\xi}\left(\xi^2\frac{d\theta}{d\xi}\right) + \theta^n = 0, \tag{16}$$

which is the Lane–Emden equation.

At the center, $\rho(0) = \rho_c$ implies $\theta(0) = 1$. To find the second initial condition $\theta'(0)$, we assume a series solution of θ and solve for the coefficients using Mathematica; the prompt is included in Appendix . We find

$$\theta(\xi) = 1 - \frac{1}{6}\xi^2 + \frac{n}{120}\xi^4 + \cdots \tag{17}$$

and thus our second initial condition is $\theta'(0) = 0$. We solve the Lane–Emden equation with $n = 1$ analytically using Mathematica (prompt in Appendix). The solution of Eq. (16) is shown in Fig. 1.

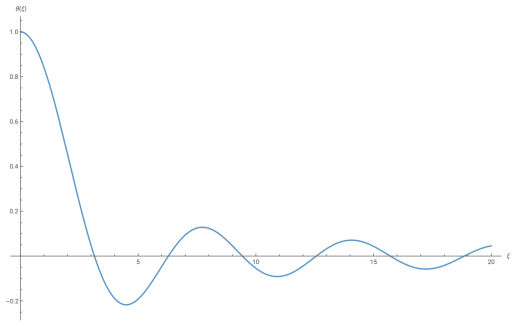

FIG. 1. Solution of the Lane–Emden equation.

We know the total mass is

$$M \equiv m(R) = \int_0^R 4\pi r^2\rho(r)\,dr. \tag{18}$$

Using the Lane–Emden variables $\rho(r) = \rho_c\theta(\xi)^n$ and $r = a\xi$ (so $dr = a\,d\xi$ and $R = a\xi_n$), we obtain

$$M = 4\pi\rho_c a^3\int_0^{\xi_n}\xi^2\theta(\xi)^n\,d\xi. \tag{19}$$

Equation (16) implies

$$\frac{d}{d\xi}\big(\xi^2\theta'(\xi)\big) = -\xi^2\theta(\xi)^n. \tag{20}$$

Integrating from 0 to ξ_n gives

$$\big[\xi^2\theta'(\xi)\big]_0^{\xi_n} = -\int_0^{\xi_n}\xi^2\theta^n\,d\xi. \tag{21}$$

Imposing $\theta'(0) = 0$ gives

$$\int_0^{\xi_n}\xi^2\theta^n\,d\xi = -\xi_n^2\theta'(\xi_n). \tag{22}$$

Substituting into Eq. (19) yields

$$M = 4\pi\rho_c a^3\left(-\xi_n^2\theta'(\xi_n)\right). \tag{23}$$

Finally, since $R = a\xi_n$ we have $a^3 = R^3/\xi_n^3$, so

$$M = 4\pi\rho_c R^3\left(-\frac{\theta'(\xi_n)}{\xi_n}\right). \tag{24}$$

Starting from Eq. (24) and using the Lane–Emden scaling $R = a\xi_n$ (so $a = R/\xi_n$) and Eq. (14) we can write ρ_c as

$$\rho_c = \left[\frac{(n+1)K}{4\pi G}\,\frac{\xi_n^2}{R^2}\right]^{\frac{n}{n-1}}. \tag{25}$$

Substituting this into Eq. (24) gives

$$M = 4\pi\left(-\frac{\theta'(\xi_n)}{\xi_n}\right)R^3\left[\frac{(n+1)K}{4\pi G}\,\frac{\xi_n^2}{R^2}\right]^{\frac{n}{n-1}} \tag{26}$$

$$= 4\pi\big[-\theta'(\xi_n)\big]\,\xi_n^{\frac{n+1}{n-1}}\left(\frac{(n+1)K}{4\pi G}\right)^{\frac{n}{n-1}}R^{\frac{n-3}{n-1}}. \tag{27}$$

Therefore,

$$M \propto R^{\frac{n-3}{n-1}} = R^{\frac{3-n}{1-n}}, \qquad (n \neq 1). \tag{28}$$

Observational mass–radius relation

With the theoretical scaling in hand, we next convert the observational measurements into radii so that the data can be compared directly to polytropic expectations.

The data provide each star's mass M (in units of $M_\odot$) and surface gravity $\log_{10}(g)$ in cgs units. Using Newtonian gravity at the stellar surface,

$$g = \frac{GM}{R^2}, \tag{29}$$

we convert the measured $(M, \log_{10} g)$ pairs into radii via

$$R = \sqrt{\frac{GM}{g}}, \qquad g = 10^{\log_{10}(g)}\ \ (\mathrm{cm\ s^{-2}}), \tag{30}$$

and then express R in Earth radii and M in solar masses. This produces an empirical M–R relation that can be directly compared to the polytropic predictions derived above. The empirical relation is shown in Fig. 2.

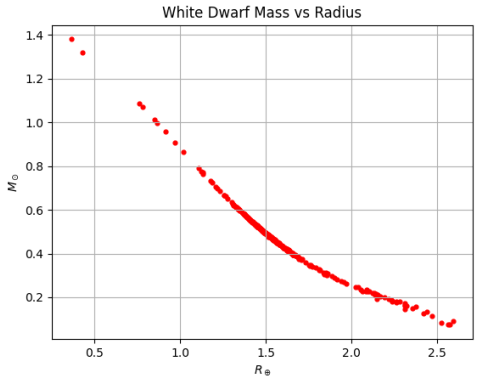

FIG. 2. White dwarf mass–radius data.

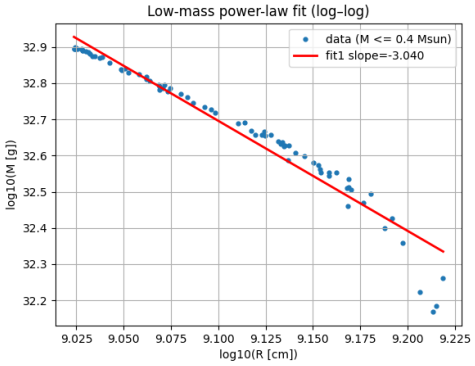

FIG. 3. Power-law fit to the low-mass white dwarf data.

Low-mass limit and polytropic fit

To connect the data with the polytropic framework, we approximate the full cold white-dwarf EOS in the low-density regime and fit the low-mass subset with a power law.

The EOS for cold white dwarfs is given by

$$P = C\left[x(2x^2-3)\left(x^2+1\right)^{1/2} + 3\sinh^{-1}x\right], \quad x = \left(\frac{\rho}{D}\right)^{1/q}. \tag{31}$$

For low-mass white dwarfs, we retain only the leading term in Eq. (31). We obtain the series expansion around $x = 0$ using Mathematica(see Appendix) as

$$C\left(\frac{8x^5}{5} - \frac{4x^7}{7} + \frac{x^9}{3} + \ldots\right). \tag{32}$$

Substituting x into the series expansion, we can write Eq. (31) as

$$P = K_*\,\rho^{1+\frac{1}{n_*}}, \tag{33}$$

where $n_* = \frac{q}{5-q}$ and $K_* = \frac{8C}{5D^{5/q}}$. Now we can use Eq. (28): the low-mass portion of the data should follow a power law. To identify the range where the power law holds, we use a log–log plot. We vary the upper mass cutoff and find that the subset $M \le 0.4\,M_\odot$ is well described by a power law. The fit is shown in Fig. 3. We first perform a linear least-squares fit in log–log space on the low-mass subset $M \le 0.4\,M_\odot$ to obtain a free slope α and intercept. This gives

$$\alpha = -3.0398. \tag{34}$$

From α we infer the effective polytropic index by inverting $\alpha = (3-n_*)/(1-n_*)$:

$$n_* = \frac{3-\alpha}{1-\alpha} = 1.4951. \tag{35}$$

The low-mass EOS relates n_* to a theory-motivated integer parameter q via

$$n_* = \frac{q}{5-q} \quad \Longleftrightarrow \quad q = \frac{5n_*}{1+n_*}. \tag{36}$$

Using the fitted n_* yields $q = 2.9961$, which rounds to the integer $q = 3$.

With q fixed to its integer value, we set

$$n_* = \frac{3}{5-3} = \frac{3}{2} = 1.5, \quad \alpha_{\text{fixed}} = \frac{3-n_*}{1-n_*} = -3, \tag{37}$$

and perform a second fit with the slope fixed to α_{fixed} to determine only the amplitude. This gives

$$A_{\text{fixed}} = 9.9084 \times 10^{59}, \tag{38}$$

where the fit is performed in CGS units (M in g and R in cm), i.e. $M = A_{\text{fixed}} R^{\alpha_{\text{fixed}}}$.

Finally, we solve the Lane–Emden equation with RK4. Using the Lane–Emden solution for $n = 3/2$, we obtain the constants

$$\xi_{\frac{3}{2}} = 3.65375379, \qquad \theta'(\xi_{\frac{3}{2}}) = -0.203301285, \tag{39}$$

which allow conversion of the fitted amplitude into the polytropic constant K_*. The resulting best-fit value is

$$K_* = 2.8227 \times 10^{12}\ \text{dyn}\,\text{cm}^{-2}\left(\text{cm}^3\,\text{g}^{-1}\right)^{5/3}. \tag{40}$$

Therefore, the low-mass white dwarf data are consistent with an effective polytropic index $n_* = 3/2$ (equivalently $q = 3$) and the fitted polytropic constant above. We then compute ρ_c using Eq. (25) and $a = \frac{R}{\xi_{\frac{3}{2}}}$ for each white dwarf in our low-mass subset. The results we obtain are shown in Fig. 4.

Full white dwarf EOS and Chandrasekhar mass

We now switch from the low-x approximation to the full EOS and use it to construct a model mass–radius curve across the observed range.

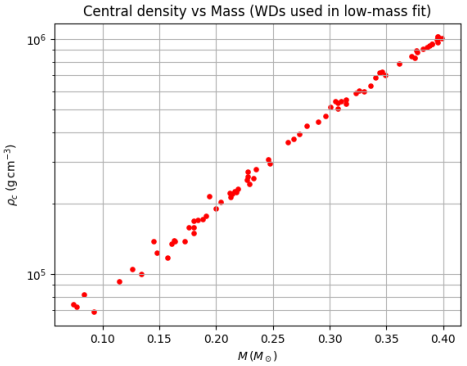

FIG. 4. ρ_c versus mass for low-mass white dwarfs.

For the full white dwarf EOS we use Eq. (31). In the low-mass regime with $q = 3$ fixed to the integer value found above, this EOS reduces to the polytropic form and the coefficients satisfy

$$K_* = \frac{8C}{5D^{5/q}}. \tag{41}$$

Therefore, once K_* and q are known from the low-mass fit, C is not an independent free parameter:

$$C(D) = \frac{5}{8} K_* D^{5/q}. \tag{42}$$

As a result, the full EOS now has only a single unknown parameter, D. For a chosen trial value of D (and thus $C(D)$), we compute the model mass–radius relation by solving the Newtonian stellar structure equations in Eq. (1) closed with the EOS (31). The integration is performed as an initial value problem (IVP): we choose a central density ρ_c and set the central boundary conditions

$$m(0) = 0, \qquad \rho(0) = \rho_c, \qquad p(0) = p(\rho_c). \tag{43}$$

We then integrate outward until the surface where $\rho(r)$ drops to zero; at that point the stellar radius and mass are

$$R = r_{\rm surf}, \qquad M = m(R). \tag{44}$$

Thus, for fixed EOS parameters, the mapping $\rho_c \mapsto (R, M)$ is obtained by a single IVP solve.

A naive approach would attempt to match each observed radius $\tilde{R}_j$ by solving $R(\rho_c) = \tilde{R}_j$ for ρ_c via root finding, which would require many IVP solves per data point and is computationally expensive. Instead, for each trial D we compute a modest number (e.g. ~ 20) of model stars by sampling central densities $\{\rho_{c,i}\}$ (chosen approximately log-uniform so that the resulting radii span the full observed radius range). This produces a set of model points

$$(R_i, M_i) = \big(R(\rho_{c,i}),\, M(\rho_{c,i})\big). \tag{45}$$

We then construct a model function $M_{\rm model}(R)$ from these samples using SciPy's cubic spline interpolation, and evaluate it at the observed radii. For each trial D we define a total mismatch between the predicted and observed masses

$$E(D) = \sum_j \left(\tilde{M}_j^{\rm pred} - \tilde{M}_j\right)^2, \tag{46}$$

and scan over a log-spaced grid of D values. In the low-mass subset ($M \le 0.4\,M_\odot$) we found

$$\rho_c \sim 7 \times 10^4\text{–}10^6 \ \text{g/cm}^3.$$

Therefore, to ensure that the low-mass objects remain in the regime $\rho/D \ll 1$ while still allowing heavier stars to approach $\rho/D \sim 1$, we scan D over a log-spaced grid in the range $D \in [10^6, 10^8]$ g/cm^3.

The best-fit EOS parameter is then chosen by

$$D_{\rm best} = \arg\min_D E(D), \tag{47}$$

with $C_{\rm best} = C(D_{\rm best})$. The error as a function of D is shown in Fig. 5. The U-shaped curve means that our scan

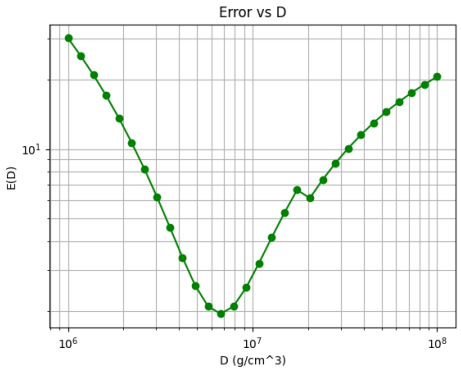

FIG. 5. Error versus D.

is finding the best-fit density scale and the minimum is at $D_{\rm best} \approx 6.72 \times 10^6$ g/cm^3, which gives $C_{\rm best} \approx 4.23 \times 10^{23}$. Comparing these with the theoretical values given by

$$C = \frac{m_e^4 c^5}{24\pi^2\hbar^3}, \quad D = \frac{m_u m_e^3 c^3 \mu_e}{3\pi^2\hbar^3}, \tag{48}$$

where $\mu_e = 2$ gives $D_{\rm best} \approx 3.45 D_{\rm theoretical}$ and $C_{\rm best} \approx 7.04 C_{\rm theoretical}$. This sounds large in percent but in astronomical units, it is still order-of-magnitude agreement.

Now that we have C, D, and q, we can plot the M versus R curve using our numerical solutions. We sweep over various ρ_c values to obtain (M, R) by solving IVPs. We report that there is a maximum possible mass $M_{\rm Ch}$ above which there is no white dwarf solution. This mass is known as the Chandrasekhar mass. The M–R curve is given in Fig. 6 with the numerical Chandrasekhar mass we calculated as $M_{\rm Ch} \approx 2.26 M_\odot$ at $R \approx 0.12 R_\odot$.

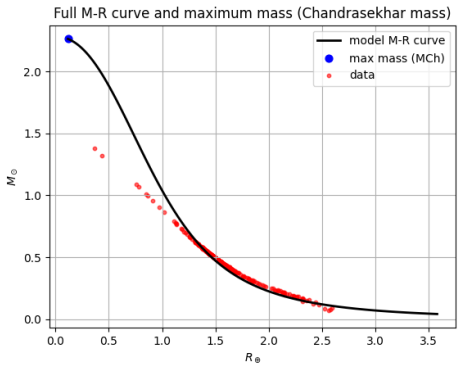

FIG. 6. Full M–R curve with C, D, and q obtained numerically.

We can also see the Chandrasekhar mass analytically by looking at the $x \gg 1$ limit in Eq. (31). Using Mathematica(prompt in Appendix), we obtain the expansion for this limit as

$$f(x) = \frac{1}{4}\left(-7 + \frac{5}{x^2} - 8x^2 + 8x^4 + 6\log(4x^2)\right) + \cdots . \tag{49}$$

In the ultra-relativistic regime $x \gg 1$, the dominant term is the x^4 term:

$$f(x) \simeq \frac{1}{4}(8x^4) = 2x^4, \tag{50}$$

so that

$$P \simeq 2C\, x^4. \tag{51}$$

For white dwarfs we use $q = 3$, hence $x = (\rho/D)^{1/3}$ and therefore $x^4 = (\rho/D)^{4/3}$. The EOS becomes

$$P \simeq 2C\left(\frac{\rho}{D}\right)^{4/3} = K_{\rm rel}\,\rho^{4/3}, \qquad K_{\rm rel} \equiv 2C\,D^{-4/3}. \tag{52}$$

This is a polytropic EOS of the form $P = K\rho^{1+1/n}$ with

$$1 + \frac{1}{n} = \frac{4}{3} \quad \Rightarrow \quad n = 3. \tag{53}$$

For a polytrope $P = K\rho^{1+1/n}$, the total mass is

$$M = 4\pi\, a^3 \rho_c \left[-\xi^2\theta'(\xi)\right]_{\xi=\xi_1}, \quad a^2 = \frac{(n+1)K}{4\pi G}\,\rho_c^{\frac{1-n}{n}}. \tag{54}$$

For $n = 3$, $a^3\rho_c = \left(\frac{4K}{4\pi G}\right)^{3/2}$ is independent of ρ_c, so the mass approaches a constant (the Chandrasekhar mass):

$$M_{\rm Ch} = 4\pi\left(\frac{K_{\rm rel}}{\pi G}\right)^{3/2}\left[-\xi^2\theta'(\xi)\right]_{\xi=\xi_1}^{(n=3)}. \tag{55}$$

Using the exact theoretical constants in Eq. (48), the ultra-relativistic polytropic constant becomes

$$K_{\rm rel} = 2C\,D^{-4/3} = 2\left(\frac{m_e^4 c^5}{24\pi^2\hbar^3}\right)\left(\frac{3\pi^2\hbar^3}{\mu_e m_u m_e^3 c^3}\right)^{4/3} \tag{56}$$

$$= \frac{1}{4}\,3^{1/3}\pi^{2/3}\,\frac{\hbar c}{(\mu_e m_u)^{4/3}}. \tag{57}$$

Substituting into the $n = 3$ mass formula gives

$$M_{\rm Ch} = 4\pi\left(\frac{1}{4}\,3^{1/3}\pi^{2/3}\right)^{3/2}\left[-\xi^2\theta'(\xi)\right]_{\xi=\xi_1}^{(n=3)}\frac{(\hbar c)^{3/2}}{G^{3/2}(\mu_e m_u)^2}. \tag{58}$$

Equivalently, grouping constants,

$$M_{\rm Ch} = \left(\frac{\sqrt{3\pi}}{2}\right)\left[-\xi^2\theta'(\xi)\right]_{\xi=\xi_1}^{(n=3)}\frac{(\hbar c)^{3/2}}{G^{3/2}(\mu_e m_u)^2}. \tag{59}$$

For the $n = 3$ Lane–Emden solution, ξ_1 and $\theta'(\xi_1)$ are fixed numbers, so $M_{\rm Ch}$ is fully determined by fundamental constants and μ_e. With $\mu_e = 2$, $M_{\rm Ch} \approx 1.46 M_\odot$. Comparing it with the one we found with our numerical curve, we have

$$M_{\rm Ch(numerical)} \approx 1.55\, M_{\rm Ch(analytical)}. \tag{60}$$

A natural next step is to see how these conclusions change once general relativity becomes essential, which we address by switching to the TOV equations for neutron stars.

EINSTEIN

In general relativity, a static, spherically symmetric star in hydrostatic equilibrium is described by the Tolman–Oppenheimer–Volkoff (TOV) equations for the enclosed gravitational mass $m(r)$ and pressure $p(r)$:

$$\frac{dm}{dr} = 4\pi r^2 \rho, \tag{61}$$

$$\frac{d\nu}{dr} = \frac{2\left(m + 4\pi r^3 p\right)}{r\left(r - 2m\right)}, \tag{62}$$

$$\frac{dp}{dr} = -\frac{\left(m + 4\pi r^3 p\right)}{r\left(r - 2m\right)}\left(\rho + p\right), \tag{63}$$

where $\rho(r)$ is the total energy density and $\nu(r)$ is the metric potential controlling gravitational time dilation via $g_{tt} = -e^{\nu}$.

To close the system we use the project equation of state (EOS),

$$p = K\rho_r^{\Gamma}, \qquad \rho = \rho_r + \frac{K}{\Gamma - 1}\rho_r^{\Gamma} = \rho_r + \frac{p}{\Gamma - 1}, \tag{64}$$

where ρ_r is the rest-mass density. The constant K is fixed by the reference condition: the EOS must satisfy

the stated pressure at $\rho_r = 10^{13}\,\mathrm{g\,cm^{-3}}$; thus for each Γ we compute

$$K(\Gamma) = \frac{p_{\rm ref}}{\rho_{r,\rm ref}^{\Gamma}}. \tag{65}$$

We solve the problem for two values of the polytropic index, $\Gamma = 1.3569$ and $\Gamma = 2.7138$, and report results for each EOS separately.

We integrate the TOV system outward from the stellar center with initial conditions

$$m(0) = 0, \qquad p(0) = p_c, \tag{66}$$

and we set $\nu(0) = 0$. This choice is without loss of generality for the mass–pressure solution because shifting $\nu \to \nu + \mathrm{const}$ does not affect the coupled equations for $m(r)$ and $p(r)$. For each chosen central pressure p_c we integrate until the surface, defined by $p(R) = 0$ (equivalently $\rho = 0$), and then record the gravitational mass $M = m(R)$ and radius R. Sweeping over a range of p_c values produces the neutron-star mass–radius curve $M(R)$ shown in Fig. 7 for each EOS.

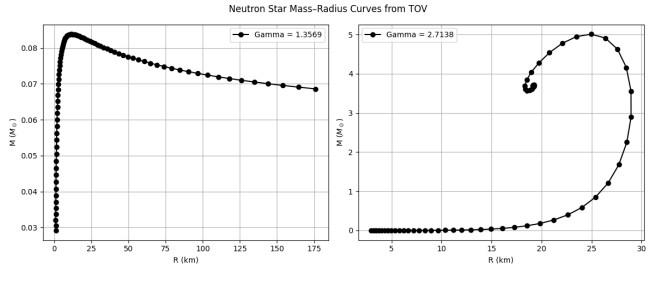

FIG. 7. Mass–radius relations $M(R)$ obtained by integrating the TOV equations outward from the stellar center to the surface, for the two polytropic equations of state with $\Gamma = 1.3569$ and $\Gamma = 2.7138$.

In addition to the gravitational mass $M = m(R)$, we compute the baryonic (rest) mass by integrating an auxiliary ODE alongside the TOV system

$$\frac{dm_P}{dr} = 4\pi \left(1 - \frac{2m}{r}\right)^{-1/2} r^2\, \rho_r, \tag{67}$$

where ρ_r is the *rest-mass* density. For each central pressure p_c, we solve the coupled system for (m, ν, p, m_P) from the center to the surface defined by $p(R) = 0$, and record $M = m(R)$ and $M_P = m_P(R)$.

From these quantities we compute the fractional binding energy

$$\Delta \equiv \frac{M_P - M}{M}, \tag{68}$$

and plot $\Delta(R)$ (Fig. 8) as well as the parametric relation M versus M_P for each equation of state (Fig. 9). The curve $M(M_P)$ can develop a cusp as the central pressure is increased. This indicates that the family of equilibrium solutions has reached a turning point where the mapping from p_c to (M_P, M) is no longer one-to-one. In particular, the cusp signals that the gravitational mass M is no longer monotonic in p_c. As a result, the maximum values of M and M_P generally occur at different central pressures, so the configuration with $M_{\rm max}$ need not coincide with the configuration with $M_{P,\rm max}$.

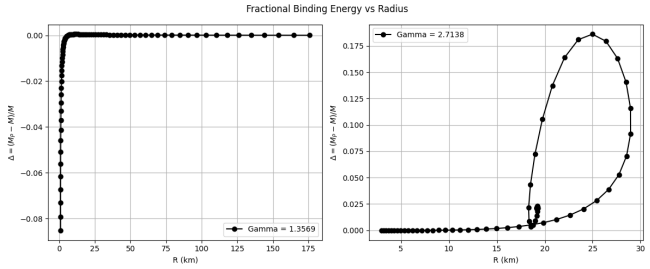

FIG. 8. Fractional binding energy Δ as a function of radius R, computed from TOV solutions with the baryonic mass $M_P = m_P(R)$ obtained by integrating the rest-mass equation using ρ_r for $\Gamma = 1.3569$ and $\Gamma = 2.7138$.

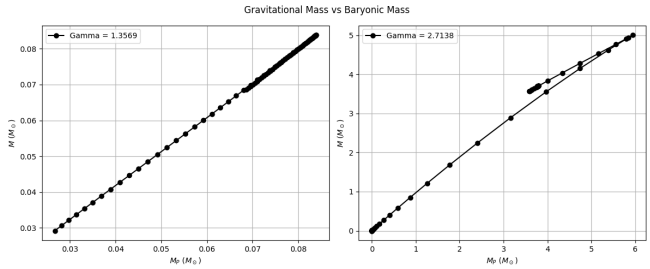

FIG. 9. Gravitational mass $M = m(R)$ versus baryonic mass $M_P = m_P(R)$ for the family of TOV solutions generated by varying the central pressure p_c (shown separately for $\Gamma = 1.3569$ and $\Gamma = 2.7138$).

The stability criterion is that configurations satisfying

$$\frac{dM}{d\rho_c} > 0 \tag{69}$$

are stable to radial perturbations, while those with $dM/d\rho_c < 0$ are unstable. Along each sequence the turning point occurs at the maximum mass $M_{\rm max}$ where $dM/d\rho_c = 0$. Therefore, we identify the stable branch as the set of models up to (and including) the configuration with $M_{\rm max}$, and the unstable branch as the continuation beyond this turning point. In Fig. 10 we show $M(\rho_c)$ on a logarithmic ρ_c axis with the stable branch plotted as a solid line and the unstable branch as a dashed line.

From the $M(\rho_c)$ sequences we obtain the maximum gravitational masses

$$\Gamma = 1.3569: \quad M_{\rm max} = 0.0838149\, M_\odot, \tag{70}$$

$$\Gamma = 2.7138: \quad M_{\rm max} = 5.00561\, M_\odot. \tag{71}$$

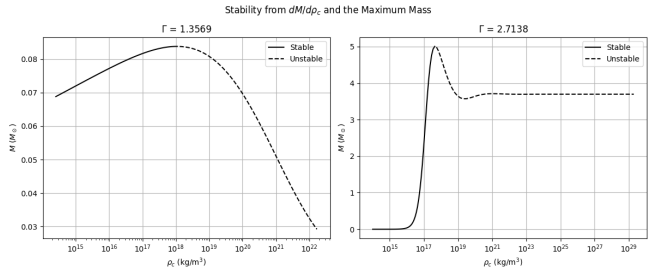

FIG. 10. Gravitational mass M as a function of central density ρ_c for the TOV sequences with $\Gamma = 1.3569$ and $\Gamma = 2.7138$.

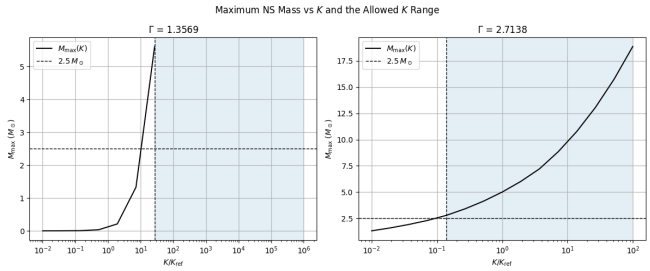

FIG. 11. Maximum gravitational mass as a function of the polytropic constant K for $\Gamma = 1.3569$ (left) and $\Gamma = 2.7138$ (right), shown versus $K/K_{\rm ref}$. The dashed horizontal line marks the requirement $M_{\max} \geq 2.5\,M_\odot$, the vertical dashed line indicates the corresponding minimum allowed K, and the shaded region shows the allowed range within the scanned interval.

We can repeat the stability plot using $M_P(\rho_c)$ because both M and M_P come from the same one-parameter sequence of stars (parameterized by p_c or ρ_c). The cusp seen in the M–M_P curve shows that M and M_P do not reach their maxima at the same central density: near the turning point where M is maximal, M begins to decrease with increasing ρ_c, while M_P is still changing differently. This is why the M–M_P curve folds back on itself (cusp). Therefore, $M_P(\rho_c)$ must also develop a turning-point behavior along the same sequence, so using M_P instead of M leads to the same qualitative separation into a pre-turning (stable) branch and a post-turning (unstable) continuation.

Keeping the polytropic index Γ fixed, we vary the polytropic constant K in the EOS $p = K\rho_r^\Gamma$ and, for each K, generate a TOV sequence by sweeping the central pressure. For each K we identify the maximum supported gravitational mass $M_{\max}(K)$ at the turning point of the sequence. Fig. 11 shows $M_{\max}$ as a function of K (plotted as the dimensionless ratio $K/K_{\rm ref}$), illustrating that larger K corresponds to a stiffer EOS and therefore a larger maximum mass.

Imposing the observational requirement that the EOS must support at least a $2.5\,M_\odot$ neutron star, we obtain the lower bounds

$$\Gamma = 1.3569: \quad \frac{K}{K_{\rm ref}} \gtrsim 26.827, \tag{72}$$

$$\Gamma = 2.7138: \quad \frac{K}{K_{\rm ref}} \gtrsim 0.13895. \tag{73}$$

Within the explored range of K, this constraint provides a minimum allowed K (no upper bound).

Outside the star ($r > R$) the fluid variables vanish ($p = \rho = 0$) and the enclosed mass becomes constant, $m(r) = M$. The ν-equation in the TOV system Eqs. (61)–(63) therefore reduces to

$$\frac{d\nu}{dr} = \frac{2M}{r(r-2M)}, \qquad r > R. \tag{74}$$

We solve this first-order ODE with the boundary condition that ν is continuous at the stellar surface,

$$\nu(R) = \nu_R. \tag{75}$$

Using the Mathematica prompt in Appendix , we find

$$\nu(r) = \nu_R + \ln(r-2M) - \ln r + \ln R - \ln(R-2M). \tag{76}$$

Combining logarithms gives

$$\ln(r-2M) - \ln r = \ln\left(1 - \frac{2M}{r}\right), \tag{77}$$

and

$$\ln(R-2M) - \ln R = \ln\left(1 - \frac{2M}{R}\right), \tag{78}$$

so the exterior metric function can be written as

$$\nu(r) = \nu_R + \ln\left(1 - \frac{2M}{r}\right) - \ln\left(1 - \frac{2M}{R}\right), \qquad r > R. \tag{79}$$

CONCLUSION

In the Newtonian part, we derived the Lane–Emden equation and the polytropic mass–radius scaling, converted the observational white dwarf catalog into an empirical M–R relation, and showed that the low-mass subset is consistent with an effective polytropic index $n_* = 3/2$ (equivalently $q = 3$) with fitted $K_* = 2.8227 \times 10^{12}$ in the stated units. Using the full cold white-dwarf EOS, a one-parameter scan over D yields $D_{\rm best} \approx 6.72 \times 10^6\,{\rm g/cm^3}$ and $C_{\rm best} \approx 4.23 \times 10^{23}$, and the numerical mass–radius curve exhibits a maximum mass identified with the Chandrasekhar limit; the numerical and analytic results differ by a factor $M_{\rm Ch(numerical)} \approx 1.55\,M_{\rm Ch(analytical)}$. In the relativistic part, integrating the TOV equations produces mass–radius and binding-energy relations for two polytropic indices and identifies stable versus unstable branches via turning points, giving $M_{\max} = 0.0838149\,M_\odot$ for $\Gamma = 1.3569$ and

$M_{\max} = 5.00561\,M_\odot$ for $\Gamma = 2.7138$. Finally, imposing $M_{\max} \geq 2.5\,M_\odot$ yields lower bounds on the stiffness parameter: $K/K_{\rm ref} \gtrsim 26.827$ for $\Gamma = 1.3569$ and $K/K_{\rm ref} \gtrsim 0.13895$ for $\Gamma = 2.7138$.

REFERENCES

[1] Fethi M. Ramazanoglu. Final project: Stars, from newton to einstein. Course handout (PDF), 2026. Provided in class.

Appendix

```
In[62]:= ClearAll["Global`*"];

(* Use x instead of the Greek letter ξ to avoid symbol issues *)
eqTimesx2[theta_] := D[x^2 D[theta, x], x] + x^2 Exp[n Log[theta]];

(* Regular-center series ansatz *)
thetaSeries = 1 + c2 x^2 + c4 x^4;

(* Series expand the Lane-Emden equation (multiplied by x^2) *)
expr = Normal@Series[eqTimesx2[thetaSeries], {x, 0, 4}] // Expand;

(* Set coefficients of x^2 and x^4 to zero *)
eqns = {
  Coefficient[expr, x, 2] == 0,
  Coefficient[expr, x, 4] == 0
};

sol = First@Solve[eqns, {c2, c4}] // Simplify;

thetaRegular = Expand[thetaSeries /. sol]

Out[68]= 1 - x^2/6 + n x^4/120
```

FIG. 12. Mathematica prompt for the regular solutions of Eq. (16) at the center.

```
,

ClearAll["Global`*"];
n = 1;
(* Lane-Emden eq *)
ode = θ''[x] + (2/x) θ'[x] + θ[x]^n == 0;
(* starting the integration at a small epsilon using the regular series *)
eps = 10^-6;
θ0 = 1 - eps^2/6 + (n eps^4)/120;   (* θ(eps) *)
θp0 = -eps/3 + (n eps^3)/30;        (* θ'(eps) *)
sol = NDSolve[
  {ode, θ[eps] == θ0, θ'[eps] == θp0},
  θ, {x, eps, 20},
  MaxSteps → Infinity
][[1]];
Plot[Evaluate[θ[x] /. sol], {x, 0, 20},
 PlotRange → All, AxesLabel → {"ξ", "θ(ξ)"}]
```

FIG. 13. Mathematica prompt for the Lane–Emden equation (Eq. (16)) with $n = 1$.

```
ClearAll["Global`*"];

(* Assumptions *)
$Assumptions = C > 0 && D > 0 && q > 0 && Element[q, Integers] && rho > 0;

Pofx[x_] := C * ( x * (2 x^2 - 3) * Sqrt[1 + x^2] + 3 * ArcSinh[x] );

(* Series expansion about x = 0 *)
ser = Series[Pofx[x], {x, 0, 9}] // Normal // FullSimplify;
Print["Series P(x) about x=0:  ", ser];

(* Extract the leading nonzero term (it turns out to be the x^5 term) *)
leadTerm = SeriesCoefficient[Pofx[x], {x, 0, 5}] * x^5 // FullSimplify;
Print["Leading term in small-x:  ", leadTerm];

(* Substitute x = (rho/D)^(1/q) *)
xrho = (rho/D)^(1/q);
Psmall = (leadTerm /. x → xrho) // FullSimplify;
Print["Leading term written as a function of rho:  ", Psmall];

(* Identify the rho-power alpha so that P ~ K* rho^alpha *)
alpha = Exponent[Psmall, rho] // FullSimplify;
Kstar = FullSimplify[Psmall / rho^alpha];

(* Match alpha = 1 + 1/n*  ->  n* = 1/(alpha - 1) *)
nstar = FullSimplify[1/(alpha - 1)];

Print["alpha (power of rho) = ", alpha];
Print["n* = ", nstar];
Print["K* = ", Kstar];
```

FIG. 14. Mathematica prompt for the series expansion of the Eq. 31

```
ClearAll[x];
f[x_] := x (2 x^2 - 3) Sqrt[1 + x^2] + 3 ArcSinh[x];

Series[f[x], {x, Infinity, 2}] // Normal // FullSimplify
```

FIG. 15. Series expansion for 31 in the limit $x \gg 1$

```
In[34]:= ClearAll[v, r, M, R, vR];

sol = DSolveValue[
  {v'[r] == (2 M)/(r (r - 2 M)), v[R] == vR},
  v,
  r,
  Assumptions → {M > 0, R > 2 M, r > R}
];

FullSimplify[sol[r], Assumptions → {M > 0, R > 2 M, r > R}]

expr = vR + Log[-2 M + r] + Log[R] - Log[r (-2 M + R)];

target = vR + Log[1 - 2 M/r] - Log[1 - 2 M/R];

FullSimplify[expr == target, Assumptions → {M > 0, R > 2 M, r > R}]
```

FIG. 16. Mathematica prompt for solving Eq. (74).